Supporting Information: Delocalisation enables efficient charge generation in organic photovoltaics, even with little to no energetic offset

Daniel Balzer and Ivan Kassal*
School of Chemistry, University of Sydney, NSW 2006, Australia
** Email: ivan.kassal@sydney.edu.au*

S1. Polaron-transformed Hamiltonian

Applying the polaron transformation (eq. (6) of the main text) to the total Hamiltonian results in the polaron-transformed Hamiltonian

$$\tilde{H} = e^S H e^{-S} = \tilde{H}_\mathrm{S} + \tilde{H}_\mathrm{B} + \tilde{H}_\mathrm{SB}. \tag{S1}$$

To evaluate this, we follow previous work [1], but adjust the equations to account for the two-particle picture. The polaron-transformed system Hamiltonian is

$$\tilde{H}_\mathrm{S} = \sum_{m,n} \tilde{E}_{mn} \left|m,n\right\rangle \left\langle m,n\right| + \sum_{m\neq m',n} \kappa^\mathrm{e}_{mm'} J^\mathrm{e}_{mm'} \left|m,n\right\rangle \left\langle m',n\right| + \sum_{m,n\neq n'} \kappa^\mathrm{h}_{nn'} J^\mathrm{h}_{mm'} \left|m,n\right\rangle \left\langle m,n'\right| + \sum_{o\neq o'} \kappa^\mathrm{xc}_{oo'} J^\mathrm{xc}_{oo'} \left|o,o\right\rangle \left\langle o',o'\right|, \tag{S2}$$

where the shifted energies are

$$\tilde{E}_{mn} = E_{mn} - \sum_k |g^\mathrm{e}_{mk}|^2/\omega_{mk} - \sum_k |g^\mathrm{h}_{nk}|^2/\omega_{nk} \quad \text{when } m \neq n \tag{S3}$$

$$\tilde{E}_{oo} = E_{oo} - \sum_k |g^\mathrm{xc}_{ok}|^2/\omega_{ok} \tag{S4}$$

and the couplings are renormalised by factors of the form

$$\kappa^z_{mm'} = \exp\left(-\frac{1}{2}\sum_k \left(\frac{\left(g^z_{mk}\right)^2}{\omega^2_{mk}} \coth\frac{\beta\omega_{mk}}{2} + \frac{\left(g^z_{m'k}\right)^2}{\omega^2_{m'k}} \coth\frac{\beta\omega_{m'k}}{2}\right)\right), \tag{S5}$$

where the superscript z can be any of 'e', 'h' or 'xc' to indicate which system-bath coupling strength $g^{\mathrm{e/h/xc}}_{mk}$ is used and $\beta = 1/k_\mathrm{B}T$ (here, we assume $T = 300\,\mathrm{K}$). The bath Hamiltonian is unchanged, $\tilde{H}_\mathrm{B} = H_\mathrm{B}$, while the polaron-transformed interaction Hamiltonian is

$$\tilde{H}_\mathrm{SB} = \sum_{m\neq m',n} J^\mathrm{e}_{mm'} \left|m,n\right\rangle \left\langle m',n\right| V^\mathrm{e}_{mm'} + \sum_{m,n\neq n'} J^\mathrm{h}_{nn'} \left|m,n\right\rangle \left\langle m,n'\right| V^\mathrm{h}_{nn'} + \sum_{o\neq o'} J^\mathrm{xc}_{oo'} \left|o,o\right\rangle \left\langle o',o'\right| V^\mathrm{xc}_{oo'}, \tag{S6}$$

where

$$V^z_{mm'} = \exp\left(\sum_k \frac{g^z_{mk}}{\omega_{mk}}\left(b^\dagger_{mk} - b_{mk}\right)\right) \exp\left(-\sum_k \frac{g^z_{m'k}}{\omega_{m'k}}\left(b^\dagger_{m'k} - b_{m'k}\right)\right) - \kappa^z_{mm'}. \tag{S7}$$

To simplify the system-bath interaction, which currently involves a sum over bath modes, we assume that all sites couple to their own baths with equal strengths ($g^\mathrm{e}_{nk} = g^\mathrm{e}_k$, $g^\mathrm{h}_{nk} = g^\mathrm{h}_k$, and $g^\mathrm{xc}_{nk} = g^\mathrm{xc}_k$), and that the discrete spectral density

$$j^z(\omega) = \sum_k \left(g^z_k\right)^2 \delta(\omega - \omega_k) \tag{S8}$$

can be replaced with a continuous one. We apply the commonly used super-Ohmic spectral density [1–4]

$$j^z(\omega) = \frac{\lambda^z}{2}\left(\frac{\omega}{\omega^z_c}\right)^3 \exp\left(-\frac{\omega}{\omega^z_c}\right) \tag{S9}$$

but it would be possible to choose more structured versions for specific organic semiconductors. These approximations reduce $\kappa^z_{mm'}$ to

$$\kappa^z_{mm'} = \kappa^z = \exp\left(-\int_0^\infty d\omega \frac{j^z(\omega)}{\omega^2} \coth\frac{\beta\omega}{2}\right). \tag{S10}$$

S2. Polaron-transformed Redfield equation

The polaron transformation reduces the system-bath coupling by moving most of the interaction into the polaron frame. This allows the remaining system-bath interaction (H_{SB}) to be treated perturbatively to second order, resulting in the secular polaron-transformed Redfield equation (sPTRE) [1]. The equations that follow are analogous to those derived for sPTRE [1], but they have been generalised for the two-particle picture. The quantum master equation describes the time evolution of polaron state populations,

$$\frac{d\rho_\nu(t)}{dt} = \sum_{\nu'} R_{\nu\nu'}\rho_{\nu'}(t), \tag{S11}$$

where the secular Redfield tensor contains rates of population transfer between every pair of polaron states. The Redfield tensor

$$R_{\nu\nu'} = 2\,\mathrm{Re}\left(\Gamma_{\nu'\nu,\nu\nu'} - \delta_{\nu\nu'}\sum_{\kappa}\Gamma_{\nu\kappa,\kappa\nu'}\right), \tag{S12}$$

consists of damping rates

$$\begin{aligned}
\Gamma_{\mu\nu,\mu'\nu'} = &\sum_{m,m',m'',m'''}\sum_{n,n'} J^{\mathrm{e}}_{mm'}J^{\mathrm{e}}_{m''m'''}\langle\mu|m,n\rangle\langle m',n|\nu\rangle\langle\mu'|m'',n'\rangle\langle m''',n'|\nu'\rangle K^{\mathrm{e,e}}_{mm',m''n'''}(\omega_{\nu'\mu'})\\
&+\sum_{m,m',m''}\sum_{n,n',n''} J^{\mathrm{e}}_{mm'}J^{\mathrm{h}}_{n'n''}\langle\mu|m,n\rangle\langle m',n|\nu\rangle\langle\mu'|m'',n'\rangle\langle m'',n''|\nu'\rangle K^{\mathrm{e,h}}_{mm',n'n''}(\omega_{\nu'\mu'})\\
&+\sum_{m,m'}\sum_{n}\sum_{o,o'} J^{\mathrm{e}}_{mm'}J^{\mathrm{xc}}_{oo'}\langle\mu|m,n\rangle\langle m',n|\nu\rangle\langle\mu'|o,o\rangle\langle o',o'|\nu'\rangle K^{\mathrm{e,xc}}_{mm',oo'}(\omega_{\nu'\mu'})\\
&+\sum_{m,m'}\sum_{n,n',n'',n'''} J^{\mathrm{h}}_{nn'}J^{\mathrm{h}}_{n''n'''}\langle\mu|m,n\rangle\langle m,n'|\nu\rangle\langle\mu'|m',n''\rangle\langle m',n'''|\nu'\rangle K^{\mathrm{h,h}}_{nn',n''n'''}(\omega_{\nu'\mu'})\\
&+\sum_{m,m',m''}\sum_{n,n',n''} J^{\mathrm{h}}_{nn'}J^{\mathrm{e}}_{m'm''}\langle\mu|m,n\rangle\langle m,n'|\nu\rangle\langle\mu'|m',n''\rangle\langle m'',n''|\nu'\rangle K^{\mathrm{h,e}}_{nn',m'm''}(\omega_{\nu'\mu'})\\
&+\sum_{m}\sum_{n,n'}\sum_{o,o'} J^{\mathrm{h}}_{nn'}J^{\mathrm{xc}}_{oo'}\langle\mu|m,n\rangle\langle m,n'|\nu\rangle\langle\mu'|o,o\rangle\langle o',o'|\nu'\rangle K^{\mathrm{h,xc}}_{nn',o'o'}(\omega_{\nu'\mu'})\\
&+\sum_{o,o',o'',o'''} J^{\mathrm{xc}}_{oo'}J^{\mathrm{xc}}_{o''o'''}\langle\mu|o,o\rangle\langle o',o'|\nu\rangle\langle\mu'|o'',o''\rangle\langle o''',o'''|\nu'\rangle K^{\mathrm{xc,xc}}_{oo',o''o'''}(\omega_{\nu'\mu'})\\
&+\sum_{m,m'}\sum_{n}\sum_{o,o'} J^{\mathrm{xc}}_{oo'}J^{\mathrm{e}}_{mm'}\langle\mu|o,o\rangle\langle o',o'|\nu\rangle\langle\mu'|m,n\rangle\langle m',n|\nu'\rangle K^{\mathrm{xc,e}}_{oo',mm'}(\omega_{\nu'\mu'})\\
&+\sum_{m}\sum_{n,n'}\sum_{o,o'} J^{\mathrm{xc}}_{oo'}J^{\mathrm{h}}_{nn'}\langle\mu|o,o\rangle\langle o',o'|\nu\rangle\langle\mu'|m,n\rangle\langle m,n'|\nu'\rangle K^{\mathrm{xc,h}}_{oo',nn'}(\omega_{\nu'\mu'}),
\end{aligned} \tag{S13}$$

where all the summation indices index sites, $\omega_{\nu'\mu'} = E_{\nu'} - E_{\mu'}$, and

$$K^{z,z'}_{mn,m'n'}(\omega) = \int_0^\infty e^{i\omega\tau}\,\langle V^z_{mn}(\tau)V^{z'}_{m'n'}(0)\rangle_B\,d\tau. \tag{S14}$$

The superscripts z and z' can be any of 'e', 'h' or 'xc' to indicate which system-bath coupling strength $g^{\mathrm{e/h/xc}}_{mk}$ is used. The last integral contains the bath correlation function

$$\langle V^z_{mn}(\tau)V^{z'}_{m'n'}(0)\rangle_B = \kappa^z\kappa^{z'}\left(e^{-\lambda_{mnm'n'}\phi^{z,z'}(\tau)} - 1\right), \tag{S15}$$

where $\lambda_{mnm'n'} = \delta_{mm'} - \delta_{mn'} + \delta_{nn'} - \delta_{nm'}$ and

$$\phi^{z,z'}(\tau) = \int_0^\infty d\omega\frac{\sqrt{j^z(\omega)j^{z'}(\omega)}}{\omega^2}\big(\cos(\omega\tau)\coth(\beta\omega/2) - i\sin(\omega\tau)\big). \tag{S16}$$

S3. dKMC approximations

The sPTRE master equation is too computationally expensive to apply to the full two-particle charge separation problem, so we apply four approximations to transform the method to dKMC. These follow our previous derivations of dKMC [5–7], but are adapted to the two-body situation. Tracking the full time-evolution according to the sPTRE (fig. S1a) has three computationally difficult steps that dKMC overcomes. First, calculating all N^{2d} polaron states involves diagonalising the $N^{2d} \times N^{2d}$ polaron-transformed system Hamiltonian $\tilde{H}_{\mathrm{S}}$, a task that scales as $O(N^{6d})$. Second, the full polaron-transformed Redfield tensor involves calculating N^{4d} rates between all pairs of N^{2d} polaron states. Finally, calculating each rate involves a sum over N^{8d} quadruples of site-pairs. In total, the sPTRE procedure scales as $O(N^{6d}) + O(N^{12d})$.

The first approximation is mapping the quantum master equation onto KMC (fig. S1b). On each of the n_{iters} realisations of disorder, rather than tracking the evolution of the full density matrix using sPTRE, we use the KMC procedure to track n_{traj} individual stochastic trajectories, which are then averaged. Each trajectory is propagated by choosing the next state probabilistically using the outgoing rates of population transfer from the current state. Therefore, instead of calculating rates between all pairs of states as in sPTRE, KMC only calculates outgoing rates at each of the n_{hops} hops, reducing the number of calculated rates from $O(N^{4d})$ to $O(N^{2d} n_{\mathrm{hops}} n_{\mathrm{traj}})$.

The second approximation is the use of hopping cutoffs (fig. S1c). Instead of calculating all outgoing rates at each hop, we only calculate rates to states that are close enough to the current state. In previous work, we calibrated a charge hopping radius r_{hop} [5] and an exciton hopping radius $r^{\mathrm{xc}}_{\mathrm{hop}}$ [7], which are the distances required to contain, on average, enough states such that the rates to them comprise more than a fraction a_{dKMC} of all rates (we set $a_{\mathrm{dKMC}} = 0.99$). In the two-particle picture, we only calculate rates from state ν to states ν' if the hop would displace the electron and the hole by a total of less than r_{hop} in expectation value. That is, we only consider those destination states ν' for which $|\mathbf{C}^{\mathrm{e}}_{\nu} - \mathbf{C}^{\mathrm{e}}_{\nu'}| + |\mathbf{C}^{\mathrm{h}}_{\nu} - \mathbf{C}^{\mathrm{h}}_{\nu'}| < r_{\mathrm{hop}}$, where the expectation value of the electron's position is $\mathbf{C}^{\mathrm{e}}_{\nu} = \langle \nu | \, \mathbf{r}^{\mathrm{e}} \, | \nu \rangle$ and likewise for the hole. In addition, if the current state is an exciton state, we also calculate

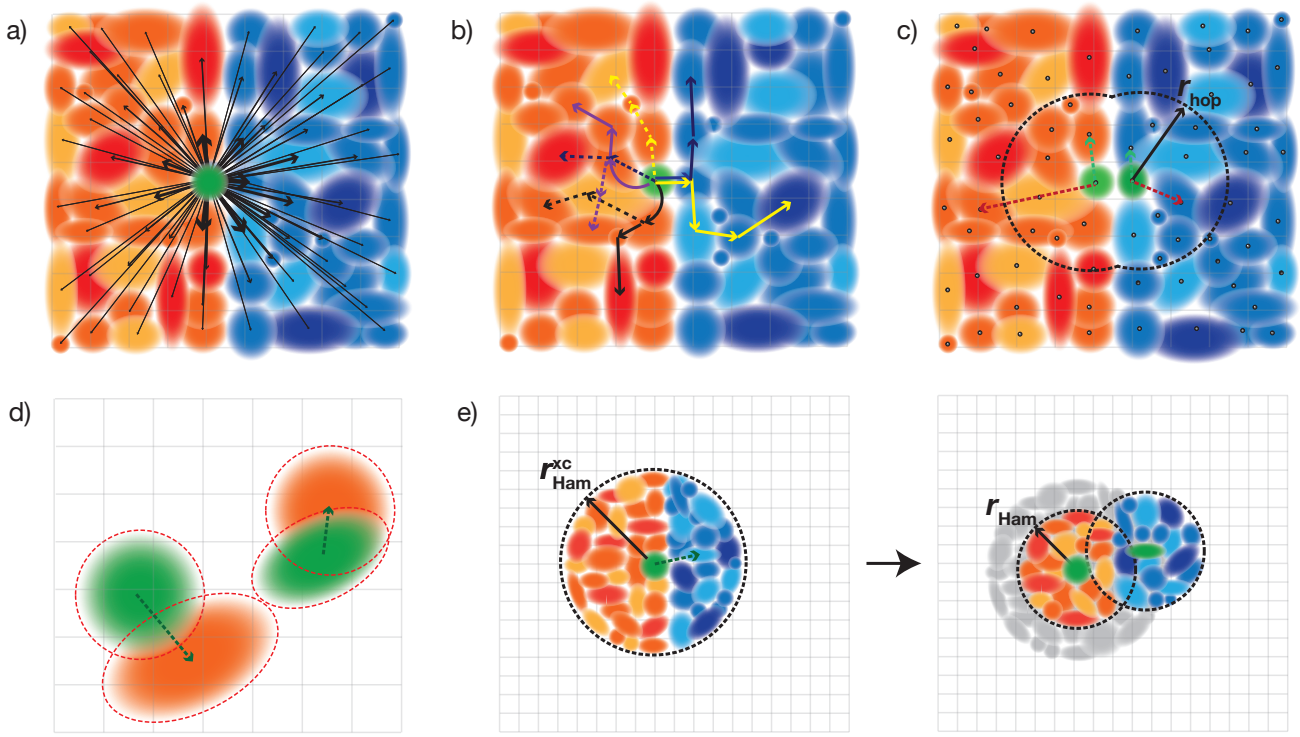

Figure S1. **Approximations of dKMC for charge generation. a)** The high computational cost of sPTRE arises from the need to track all possible transitions (black arrows) in the time-dependent evolution of the populations of all polaron states. To avoid this cost, dKMC makes the following four approximations. **b)** Kinetic Monte Carlo: we map the quantum master equation onto KMC, which propagates and averages many individual trajectories formed from sequential hops from the current state (in green), chosen probabilistically. Straight arrows denote electron (solid) and hole (dashed) hops, while curved arrows denote exciton hops. **c)** Hopping radius: we only calculate hopping rates to polaron states where the electron and the hole, or the exciton, are sufficiently close to their current positions. In the diagram, the hop depicted by the green arrows is allowed, and the red one is not. **d)** Population cutoff: in each rate calculation from the current state (both the electron and the hole depicted in green) to a possible destination state (in orange), we ignore contributions from site-pairs whose overlap with the initial or final states is insignificant, depicted as lattice points outside the dotted red outlines. **e)** Diagonalising on the fly: rather than calculating all polaron states, we only calculate them for small subsystems surrounding the electron and hole, or exciton, after each hop.

rates to all exciton states whose position $\mathbf{C}^{\mathrm{xc}}_{\nu'} = \langle \nu' | \mathbf{r}^{\mathrm{xc}} | \nu' \rangle$ is within $r^{\mathrm{xc}}_{\mathrm{hop}}$ of the current state's position $\mathbf{C}^{\mathrm{xc}}_{\nu}$. This is required because exciton states are typically more delocalised and can hop further due to longer-range dipole-dipole coupling. Overall, imposing the hopping cutoffs reduces the number of rates calculated at each hop from $O(N^{2d})$ to $O(r^{2d}_{\mathrm{hop}})$.

The third approximation is including a site-pair contribution cutoff when calculating each hopping rate (fig. S1d). Instead of including all site-pairs in the sums defining the damping rates of eq. (S13), we ignore contributions of site-pairs with insignificant overlaps with either the initial or final states. For each summation index of eq. (S13), we only include the minimum number of site-pairs (m, n) that together support at least a fraction a_{dKMC} of the population of ν or ν', as appropriate (we set $a_{\mathrm{dKMC}} = 0.99$). Ignoring contributions from site-pairs with small amplitude significantly reduces the cost of calculating each rate. However, as the spatial extent of a state is difficult to predict in general, estimating the reduction in scaling is difficult. By assuming that the each state is appreciably delocalised across not more than than r^{2d}_{hop} site-pairs, the cost for each rate calculation is no more than $O(r^{8d}_{\mathrm{hop}})$, down from $O(N^{8d})$.

The fourth and final approximation is diagonalising $\tilde{H}_S$ on the fly (fig. S1e). Instead of diagonalising the Hamiltonian describing all site-pairs, we diagonalise Hamiltonians representing subsystems, i.e., only containing site-pairs in which both the electron and the hole are close enough to their current locations. After every hop, a new subset of the original $\tilde{H}_S$ is diagonalised for the subsystem surrounding the new locations of the charges. In previous work, we calibrated Hamiltonian radii r_{Ham} and $r^{\mathrm{xc}}_{\mathrm{Ham}}$, which represent how large a subsystem Hamiltonian is required to calculate outgoing rates to a desired accuracy a_{dKMC} [5, 7]. In the two-particle picture, we only include site-pairs (m, n) whose combined distance from the current locations of the electron and the hole is within r_{Ham}, $|\mathbf{r}_m - \mathbf{C}^{\mathrm{e}}_{\nu}| + |\mathbf{r}_n - \mathbf{C}^{\mathrm{h}}_{\nu}| < r_{\mathrm{Ham}}$. In addition, if the current state is classified as an exciton, we also include exciton site-pairs (o, o) within a larger exciton Hamiltonian radius $r^{\mathrm{xc}}_{\mathrm{Ham}}$ of the exciton, i.e., $|\mathbf{r}_o - \mathbf{C}^{\mathrm{xc}}_{\nu}| < r^{\mathrm{xc}}_{\mathrm{Ham}}$. Only diagonalising subsystems reduces the cost of finding the required polaron states from $O(N^{6d})$ to $O(r^{6d}_{\mathrm{Ham}} n_{\mathrm{hops}} n_{\mathrm{traj}})$. In practice, we calculate the Hamiltonian and hopping radii simultaneously, using the same accuracy (here chosen to be $a_{\mathrm{dKMC}} = 0.99$), using the procedure outlined in previous work [7]. The choice of $a_{\mathrm{dKMC}} = 0.99$ is benchmarked in previous work, where the chosen accuracy is shown to be sufficient to converge single-particle charge mobilities [5] and exciton diffusion coefficients [7].

Overall, the four approximations described above reduce the scaling from $O(N^{6d}) + O(N^{12d})$ to $O(r^{6d}_{\mathrm{Ham}} n_{\mathrm{hops}} n_{\mathrm{traj}}) + O(n_{\mathrm{hops}} n_{\mathrm{traj}} r^{2d}_{hop} r^{8d}_{\mathrm{hop}})$. For exmaple, for the largest system we study ($d = 3$, $N = 100$, $\mu = 3\,\mathrm{D}$, $J = 22.5\,\mathrm{meV}$), dKMC reduces the computational complexity of calculations by 54 orders of magnitude over sPTRE.

S4. Recombination

Recombination of excitons and CT states is typically treated using constant rates $R^{\mathrm{xc}}_{\mathrm{recomb}}$ and $R^{\mathrm{CT}}_{\mathrm{recomb}}$ in classical kinetic Monte Carlo. That is, whenever the electron and the hole are on the same site, they can recombine with rate $R^{\mathrm{xc}}_{\mathrm{recomb}}$, and when they are on neighbouring sites, they can recombine with rate $R^{\mathrm{CT}}_{\mathrm{recomb}}$.

In dKMC, we use Fermi's golden rule to calculate the corresponding exciton and CT recombination rates from a delocalised polaron state ν [6]. The golden-rule rate for exciton recombination,

$$k^{\nu}_{\mathrm{xc,recomb}} = 2\pi \left| \sum_{o} \langle \nu | o, o \rangle \, \langle o, o | H | g \rangle \right|^2 \rho_{\mathrm{recomb}}, \tag{S17}$$

involves a sum over exciton site-pairs (where the electron and hole are on the same site) and the density of states ρ_{recomb}. If the exciton site-pairs are all equally coupled to the ground state with strength $\langle m, n | H | g \rangle = J^{\mathrm{xc}}_{\mathrm{recomb}}$, the exciton recombination rate becomes the standard Monte-Carlo rate adjusted by a delocalisation correction,

$$k^{\nu}_{\mathrm{xc,recomb}} = R^{\mathrm{xc}}_{\mathrm{recomb}} \left| \sum_{o} \langle \nu | o, o \rangle \right|^2, \tag{S18}$$

where $R^{\mathrm{xc}}_{\mathrm{recomb}} = 2\pi |J^{\mathrm{xc}}_{\mathrm{recomb}}|^2 \rho_{\mathrm{recomb}}$.

The same approach for CT-state recombination leads to

$$k^{\nu}_{\mathrm{CT,recomb}} = R^{\mathrm{CT}}_{\mathrm{recomb}} \left| \sum_{(m,n) \in \mathrm{CT}} \langle \nu | m, n \rangle \right|^2, \tag{S19}$$

where the sum is over CT site-pairs.

The constant recombination rate modified by the square of the sum of the amplitudes on relevant site-pairs agrees with generalised Marcus theory [8] and with earlier recombination studies [9]. In this work, we use $R^{\mathrm{xc}}_{\mathrm{recomb}} = 10^{-11}\,\mathrm{s}^{-1}$ and $R^{\mathrm{CT}}_{\mathrm{recomb}} = 10^{-10}\,\mathrm{s}^{-1}$.

S5. dKMC algorithm

We summarise the steps involved in the dKMC algorithm in algorithm S1.

Given parameters d, N, σ, σ_{xc}, J_{e}, J_{h}, μ, λ, λ_{xc}, E_b, ω_c, T, $R^{\mathrm{xc}}_{\mathrm{recomb}}$, R^{CT}_{recomb}, a_{dKMC}, r_{sep}, $d^{\mathrm{max}}_{\mathrm{xc}}$, n_{hops}, n_{iter}, and n_{traj}:

1. Calculate calibrating cutoff radii r_{hop} and r_{Ham} for charges and $r^{\mathrm{xc}}_{\mathrm{hop}}$ and $r^{\mathrm{xc}}_{\mathrm{Ham}}$ for excitons, using the procedure described in [7].
2. For n_{iter} realisations of disorder:
   a. Generate N^d lattice of sites, with randomly oriented dipoles $\boldsymbol{\mu}$ and HOMO and LUMO energies drawn from the bivariate normal distributions in eq. (1) of the main text.
   b. Set $n_{\mathrm{sep}} \leftarrow 0$.
   c. For n_{traj} trajectories:
      i. Choose the initial excitation location at a randomly chosen initial excitation distance $d_{\mathrm{xc}} \in [1, d^{\mathrm{max}}_{\mathrm{xc}}]$ from the interface.
      ii. Create a polaron-transformed $\tilde{H}_S$ containing all site-pairs within a combined distance of r_{Ham} of the chosen excitation location and all exciton site-pairs within $r^{\mathrm{xc}}_{\mathrm{Ham}}$. Diagonalise $\tilde{H}_S$ to find the polaron states and their energies, and calculate the expectation values of the positions of electron $\mathbf{C}^{\mathrm{e}}$, hole $\mathbf{C}^{\mathrm{h}}$, and exciton $\mathbf{C}^{\mathrm{xc}}$ in every state.
      iii. Create a list L^{xc} of exciton states (those with populations on exciton site-pairs greater than $p^{\mathrm{xc}}_{\mathrm{cutoff}}$) whose position is within 1 site of the excitation location.
      iv. Calculate the oscillator strength of each state in L^{xc} as the square of the expectation value of its transition dipole moment.
      v. Choose the initial state ν from L^{xc} probabalistically in proportion to the states' oscillator strengths.
      vi. For n_{hops} hops:
         A. If ν is an exciton state:
            - Diagonalise a new $\tilde{H}_S$, being a submatrix of the original $\tilde{H}_S$ describing site-pairs (m, n) such that $|\mathbf{r}_m - \mathbf{C}^{\mathrm{e}}_\nu| + |\mathbf{r}_n - \mathbf{C}^{\mathrm{h}}_\nu| < r_{\mathrm{Ham}}$ and (o, o) such that $|\mathbf{r}_o - \mathbf{C}^{\mathrm{xc}}_\nu| < r^{\mathrm{xc}}_{\mathrm{Ham}}$.
            - Create a list L containing states ν' such that $|\mathbf{C}^{\mathrm{e}}_\nu - \mathbf{C}^{\mathrm{e}}_{\nu'}| + |\mathbf{C}^{\mathrm{h}}_\nu - \mathbf{C}^{\mathrm{h}}_{\nu'}| < r_{\mathrm{hop}}$, and exciton states ν' such that $|\mathbf{C}^{\mathrm{xc}}_\nu - \mathbf{C}^{\mathrm{xc}}_{\nu'}| < r^{\mathrm{xc}}_{\mathrm{hop}}$.

            Else:
            - Diagonalise a new $\tilde{H}_S$, being a submatrix of the original $\tilde{H}_S$ describing site-pairs (m, n) such that $|\mathbf{r}_m - \mathbf{C}^{\mathrm{e}}_\nu| + |\mathbf{r}_n - \mathbf{C}^{\mathrm{h}}_\nu| < r_{\mathrm{Ham}}$.
            - Create a list L of all states ν' such that $|\mathbf{C}^{\mathrm{e}}_\nu - \mathbf{C}^{\mathrm{e}}_{\nu'}| + |\mathbf{C}^{\mathrm{h}}_\nu - \mathbf{C}^{\mathrm{h}}_{\nu'}| < r_{\mathrm{hop}}$.

         B. Calculate $R_{\nu\nu'}$ for all $\nu' \in L$ using eq. (S12), only summing over each index in eq. (S13) the minimum number of site-pairs (m, n) that together support at least a_{dKMC} of the population of ν or ν'.
         C. Calculate $k^{\nu}_{\mathrm{recomb}} = k^{\nu}_{\mathrm{xc,recomb}} + k^{\nu}_{\mathrm{CT,recomb}}$ using eq. (S18) and eq. (S19), and append g to L.
         D. Set $S_{\nu'} \leftarrow \sum_{\mu=1}^{\nu'} R_{\nu\mu}$ for all $\nu' \in L$ and set $W \leftarrow \sum_{\nu' \in L} S_{\nu'}$.
         E. Find ν' such that $S_{\nu'-1} < uW < S_{\nu'}$, for uniform random number $u \in (0, 1]$, and update $\nu \leftarrow \nu'$.
         F. Update $t \leftarrow t + \Delta t$, where $\Delta t = -W^{-1} \ln v$ for uniform random number $v \in (0, 1]$.
         G. If $\nu = g$, exit the for loop.
         H. If $|\mathbf{C}^{\mathrm{e}}_\nu - \mathbf{C}^{\mathrm{h}}_\nu| > r_{\mathrm{sep}}$, set $n_{\mathrm{sep}} \leftarrow n_{\mathrm{sep}} + 1$ and exit the for loop.
   d. Calculate IQE $= n_{\mathrm{sep}}/n_{\mathrm{traj}}$.
3. Calculate mean IQE by averaging all IQEs.

Algorithm S1. **dKMC for charge generation.**

S6. Parameters

Table S1 contains the parameter values used in dKMC simulations throughout this work, unless otherwise stated.

Parameter	Description	Values
d	Dimension	1–3
N	Sites along each dimension	100
σ	Electronic disorder	150 meV
σ_{xc}	Exciton disorder	30 meV
J^{e}	Electron coupling	7.5–75 meV
J^{h}	Hole coupling	7.5–75 meV
μ	Transition dipole moment	1–10 D
λ	Electronic bath reorganisation energy	100 meV
λ_{xc}	Exciton bath reorganisation energy	100 meV
E_g	HOMO-LUMO gap	1600 meV
E_b	Exciton binding energy	700 meV
$E_{\mathrm{offset}}^{\mathrm{HOMO}}$	HOMO energetic offset	500 meV
$E_{\mathrm{offset}}^{\mathrm{LUMO}}$	LUMO energetic offset	500 meV
a	Lattice spacing	1 nm
ε_r	Dielectric constant	3.5
ω_c	Bath cutoff frequency	62 meV
T	Temperature	300 K
$R_{\mathrm{recomb}}^{\mathrm{xc}}$	Exciton recombination rate	10^{-11} s^{-1}
$R_{\mathrm{recomb}}^{\mathrm{CT}}$	CT recombination rate	10^{-10} s^{-1}
a_{dKMC}	dKMC accuracy	0.99
r_{sep}	Concluding separation	5 nm
$d_{\mathrm{xc}}^{\mathrm{max}}$	Maximum excitation distance	5 nm
n_{hops}	Maximum hop number	2000
n_{iter}	Simulation landscapes	1000
n_{traj}	Trajectories on each landscape	10 in 2D, 1 in 3D

Table S1. **Parameter values.** Default values used for parameters in dKMC simulations, unless otherwise specified.

S7. Properties of polaron states

Figure S2 shows the relationship between the IPR and the energy $\tilde{E}$ of the states for small couplings and dipole moments (fig. S2a) and larger ones (fig. S2b). Figure S2a shows that when the couplings and dipole moments are small, the states are mostly localised onto one site-pair. For higher couplings and dipole moments, as in fig. S2b, the states can delocalised over more site-pairs. The IPR is greatest in the middle of the density of states, and smallest at the edges, where trap states tend to be localised. There are three peaks in the density of states due to the energetic offsets at the interface: the lowest-energy peak corresponds to the electron in the donor and the hole in the acceptor, the middle peak corresponds to the electron and hole in the same phase, and the highest-energy peak corresponds to the electron in the donor and the hole in the donor. Furthermore, as the states delocalise, they can form a significant number of hybridised states, seen as stars and squares in fig. S2b, while none form in the localised case of fig. S2a.

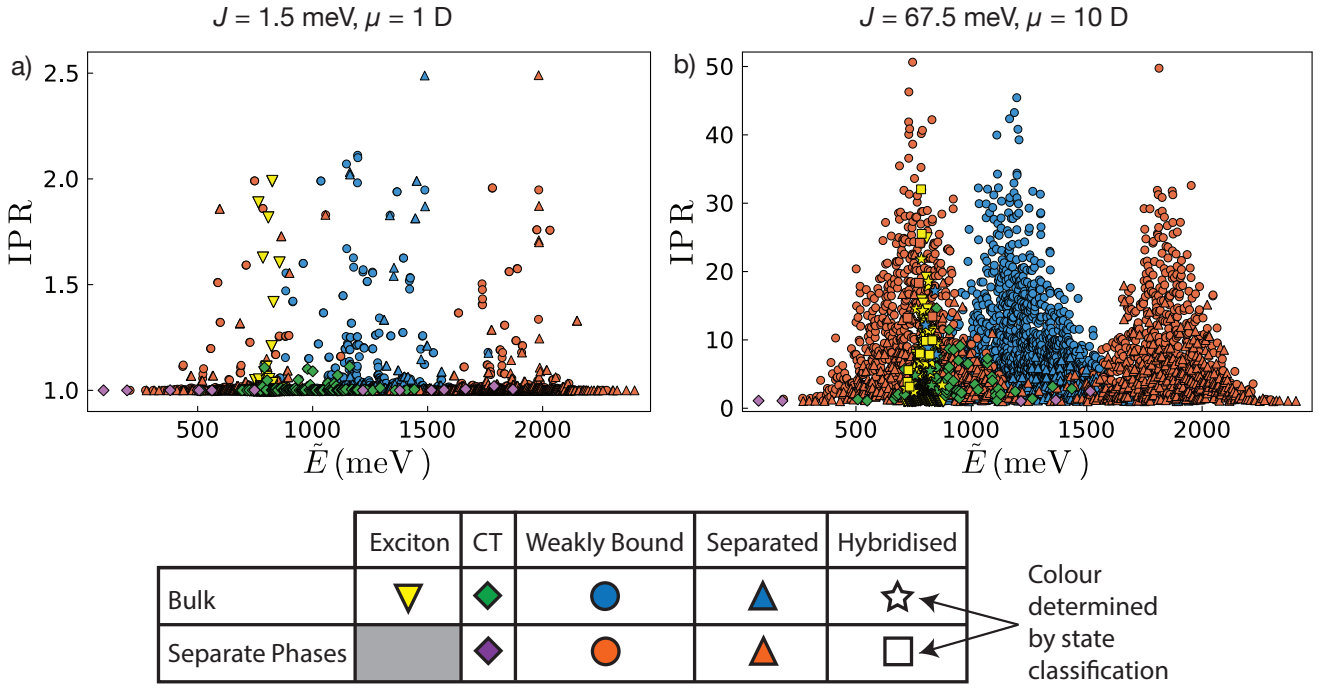

Figure S2. **Properties of the polaron states.** The inverse participation ratio (IPR) as a function of the energy $\tilde{E}$ of polaron states found by diagonalising a subset of the 2D polaron-transformed system Hamiltonian with **a)** small electronic couplings and transition dipole moments ($J = 1.5\,\text{meV}$, $\mu = 1\,\text{D}$) and **b)** large ones ($J = 67.5\,\text{meV}$, $\mu = 10\,\text{D}$). Each state is labelled based on which category of site-pair it has the greatest overlap with and whether the site-pairs are in the bulk (same phase) or different phases.

S8. Mechanisms of delocalisation enhancements

Here, we break down the mechanistic analysis of section II.D of the main text to show that the mechanisms of delocalisation enhancement are the same for both interfacial and bulk exciton dissociation. To do so, instead of looking at all separated trajectories together, we separately analyse the trajectories where the exciton dissociates at the interface (fig. S3) and those where it dissociates in the bulk, without an interfacial energetic offset (fig. S4). In both cases, the same trends are seen as in fig. 7 of main text, i.e., that delocalisation both helps charges hop further out of an exciton and form hybridised states.

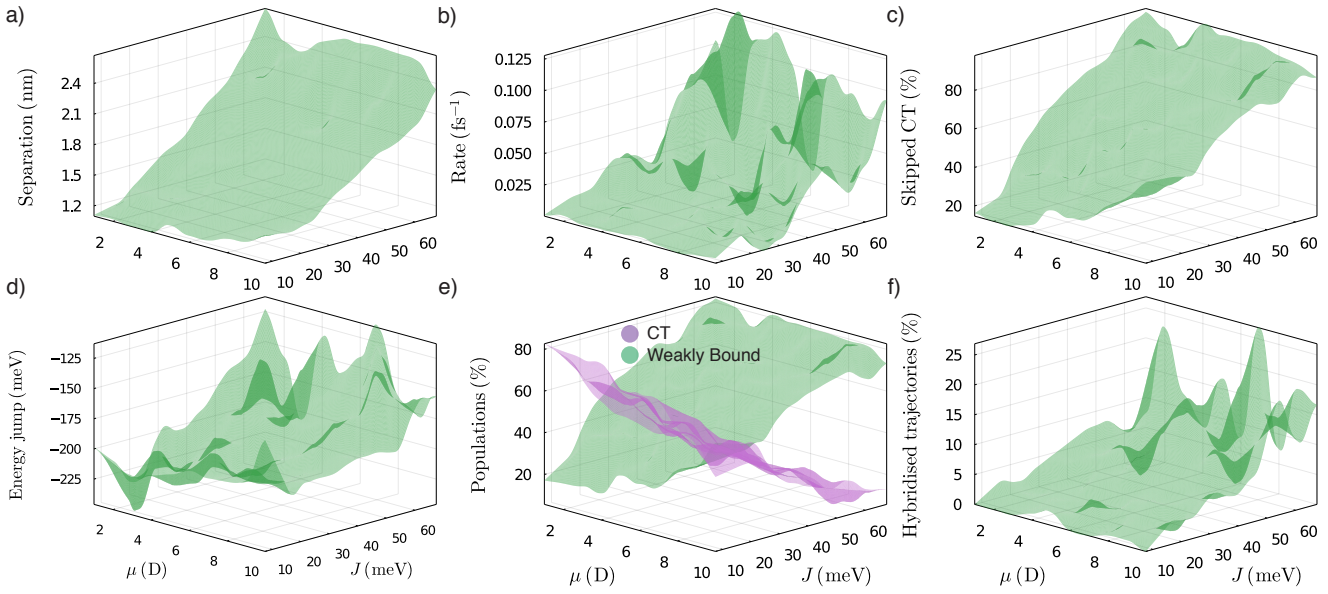

Figure S3. The same mechanistic analysis as in fig. 7 of the main text, but only for trajectories where the exciton dissociates across the interface.

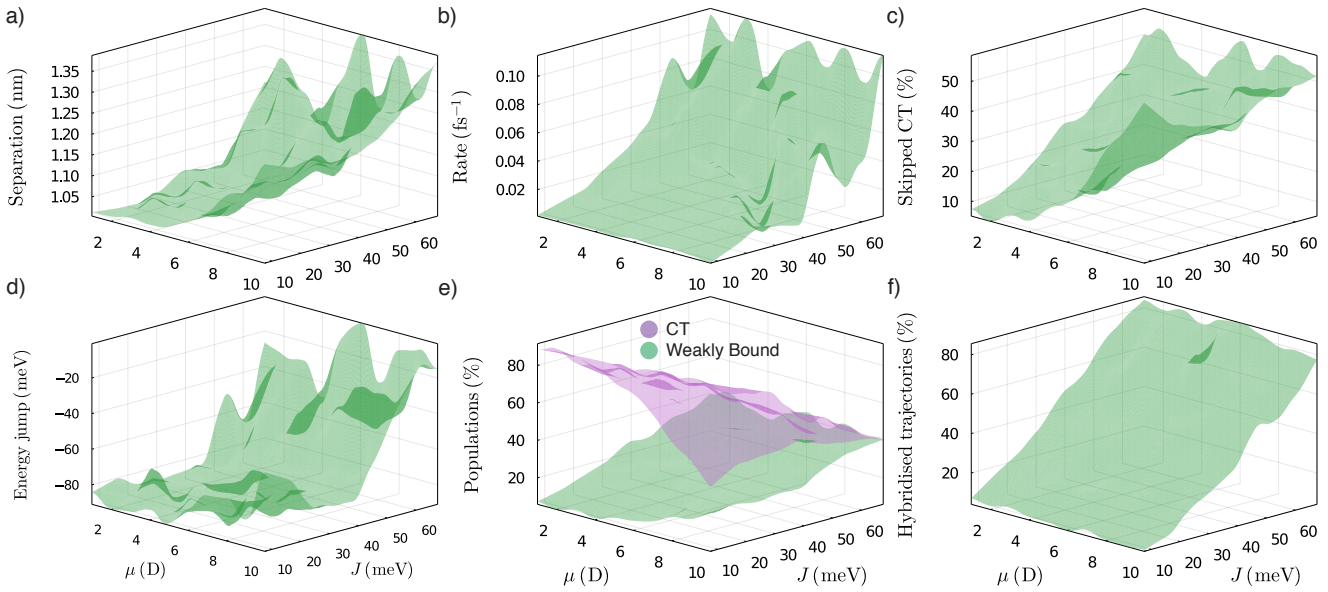

Figure S4. The same mechanistic analysis as in fig. 7 of the main text, but only for trajectories where the exciton dissociates in the bulk, without an interfacial energetic offset.

[1] C. K. Lee, J. Moix, and J. Cao, Coherent quantum transport in disordered systems: A unified polaron treatment of hopping and band-like transport, J. Chem. Phys. **142**, 164103 (2015).
[2] S. Jang, J. Cao, and R. J. Silbey, On the temperature dependence of molecular line shapes due to linearly coupled phonon bands, J. Phys. Chem. B **106**, 8313 (2002).
[3] S. Jang, Theory of multichromophoric coherent resonance energy transfer: A polaronic quantum master equation approach, J. Chem. Phys. **135**, 034105 (2011).
[4] F. A. Pollock, D. P. McCutcheon, B. W. Lovett, E. M. Gauger, and A. Nazir, A multi-site variational master equation approach to dissipative energy transfer, New J. Phys. **15**, 075018 (2013).
[5] D. Balzer, T. J. A. M. Smolders, D. Blyth, S. N. Hood, and I. Kassal, Delocalised kinetic Monte Carlo for simulating delocalisation-enhanced charge and exciton transport in disordered materials, Chem. Sci. **12**, 2276 (2021).
[6] D. Balzer and I. Kassal, Even a little delocalization produces large kinetic enhancements of charge-separation efficiency in organic photovoltaics, Sci. Adv. **8**, eabl9692 (2022).
[7] D. Balzer and I. Kassal, Mechanism of delocalization-enhanced exciton transport in disordered organic semiconductors, J. Phys. Chem. Lett. **14**, 2155 (2023).
[8] N. B. Taylor and I. Kassal, Generalised Marcus theory for multi-molecular delocalised charge transfer, Chem. Sci. **9**, 2942 (2018).
[9] R. Tempelaar, L. J. A. Koster, R. W. A. Havenith, J. Knoester, and T. L. C. Jansen, Charge recombination suppressed by destructive quantum interference in heterojunction materials, J. Phys. Chem. Lett. **7**, 198 (2016).